Chemical Physics 375 (2010) 445–449

Contents lists available at ScienceDirect

Chemical Physics

journal homepage: www.elsevier.com/locate/chemphys

Inertial Brownian motors driven by biharmonic signals

Lukasz Machura, Marcin Kostur, Jerzy Łuczka *

Institute of Physics, University of Silesia, 40-007 Katowice, Poland

ARTICLE INFO

Article history:
Received 18 January 2010
In final form 9 March 2010
Available online 15 March 2010

On the occasion of 60th birthday of Prof. Peter Hänggi

Keywords:
Transport
Brownian motors
Josephson junctions

ABSTRACT

We study transport properties of an inertial Brownian particle moving in viscous symmetric periodic structures and driven by an oscillating signal of two harmonic components. We analyze the influence of symmetric, antisymmetric and asymmetric signals on directed transport and reveal the shift symmetry of the stationary averaged velocity of the Brownian particle with respect to the relative phase of two components of the signal. The shift symmetry holds true in all regimes.

1. Introduction

Recent progress in the highly controlled fabrication of small structures opens new prospects for miniaturization of devices, machines, engines, etc. Processes in such systems can exhibit radically different properties than at the macroscopic level. For example at the microscopic scale, immanently there is a world of fluctuations which cannot be eliminated or even reduced. However, it can be exploited. A good example are biological motors like kinesin or dynein which exploit thermal fluctuations for their directed movement by the ratchet mechanism [1]. At the microscopic or mesoscopic levels, ways and means of generation and control of particle transport are important issues for both theorists [2] and experimentalists [3]. In literature, there are many suggestions and examples how to generate a directed movement of particles [2,4]. Much more difficult problem is related to a precise control of transport. In the paper, we study an archetype of transport in (spatially) periodic systems which is described by a Langevin equation. In this modeling, we know what conditions have to be fulfilled in order to generate a directed motion of a Brownian particle. Moreover, properties of this system can be experimentally verified in a setup consisting of a resistively and capacitively shunted Josephson junction device [5–7]. It is possible because the underlying dynamics can conveniently be described by an equivalent equation of motion in the Stewart–McCumber model [8–11]. In our previous papers [5,6], we have studied the system driven by a time-periodic force $G(t)$ which is the simplest harmonic signal $G(t) = A\cos(\Omega t)$ (or $G(t) = A\sin(\Omega t)$), where A and Ω are the amplitude and angular frequency of the signal, respectively. We have shown that, when additionally a constant force F is applied, anomalous transport in experimentally wide regimes can be observed: absolute negative mobility near zero value of F (a linear response regime), negative mobility in the nonlinear response regime and negative differential mobility. In this paper we extend the analysis by considering the biharmonic driving. However, we assume that the constant force $F = 0$.

The paper is organized as follows. In Section 2, we present the Langevin equation determining dynamics of the Brownian particle in presence of δ-correlated thermal fluctuations. Next, in Section 3, we address the problem of influence of the second harmonics on transport of the Brownian particle. In the parameter space, we reveal reach transport behavior. Section 4 provides summary and some conclusions.

2. Langevin dynamics

We study the motion of a classical particle of mass m moving in the periodic, symmetric one-dimensional potential $V(x) = \Delta V \sin(2\pi x/L)$ of the period L and a barrier height $2\Delta V$. The particle is driven by an unbiased time-periodic *biharmonic* force

$$G(t) = A[\sin(\Omega t) + \epsilon \sin(2\Omega t + \phi)], \tag{1}$$

where ϵ is the ratio of the second harmonic amplitude to the fundamental amplitude A and the relative phase ϕ determines the time symmetry of the system. Additionally, the particle is subjected to the thermal noise. Dynamics of a such defined Brownian motor is governed by the Langevin equation for the coordinate $x = x(t)$ of the Brownian particle which has the form [12]

* Corresponding author. Tel.: +48 32 359 11 73.
E-mail address: jerzy.luczka@us.edu.pl (J. Łuczka).
URL: http://fizyka.us.edu.pl

0301-0104/$ - see front matter © 2010 Elsevier B.V. All rights reserved.
doi:10.1016/j.chemphys.2010.03.008

$$m\ddot{x} + \gamma\dot{x} = -V'(x) + G(t) + \sqrt{2\gamma kT}\xi(t), \tag{2}$$

where the dot denotes a differentiation with respect to time and prime denotes a differentiation with respect to the argument of the potential $V(x)$. The parameter γ is the friction coefficient, T denotes temperature, and k is the Boltzmann constant. Thermal fluctuations are modeled by the zero-mean Gaussian white noise $\xi(t)$ with the correlation function $\langle\xi(t)\xi(s)\rangle = \delta(t-s)$.

We introduce dimensionless variables. The natural length scale is determined by the period L of the potential $V(x)$. The dynamics possesses several time scales. We define the characteristic time τ_0 determined from the Newton equation, $m\ddot{x} = -V'(x)$, by inserting characteristic quantities, namely, $mL/\tau_0^2 = \Delta V/L$; hence $\tau_0^2 = mL^2/\Delta V$. The dimensionless variables thus read:

$$\hat{x} = \frac{x}{L}, \quad \hat{t} = \frac{t}{\tau_0}. \tag{3}$$

The dimensionless Langevin dynamics consequently assumes the form

$$\ddot{\hat{x}} + \hat{\gamma}\dot{\hat{x}} = -\widehat{V}'(\hat{x}) + g(\hat{t}) + \sqrt{2\hat{\gamma}D_0}\hat{\xi}(\hat{t}), \tag{4}$$

where

- the re-scaled friction coefficient $\hat{\gamma} = (\gamma/m)\tau_0$ is the ratio of the two characteristic time scales, τ_0 and the relaxation time scale of the velocity degree of freedom, i.e., $\tau_L = m/\gamma$,
- the re-scaled potential

$$\widehat{V}(\hat{x}) = V(x)/\Delta V = \sin(2\pi\hat{x}) \tag{5}$$

  assumes the period 1 and the barrier height 2,
- the scaled external time-periodic force

$$g(\hat{t}) = a[\sin(\omega\hat{t}) + \varepsilon\sin(2\omega\hat{t} + \phi)], \tag{6}$$

  where the signal has the re-scaled amplitudes $a = AL/\Delta V$ and $\varepsilon = \epsilon/\Delta V$ and the dimensionless angular frequencies $\omega = \Omega\tau_0$,
- the re-scaled, zero-mean Gaussian white-noise forces $\hat{\xi}(\hat{t})$ obey $\langle\hat{\xi}(\hat{t})\hat{\xi}(\hat{s})\rangle = \delta(\hat{t}-\hat{s})$ with a re-scaled noise intensity $D_0 = kT/\Delta V$.

In the following, mostly for the sake of simplicity, we shall use only dimensionless variables and shall omit the "hat"-notation in all quantities.

Transport properties in systems driven by this type of external stimulus have been theoretically studied mainly in the overdamped regime [13–15], for moderate damping [16], both experimentally and theoretically for cold atoms in the optical lattices [17–19], and for driven Josephson junctions [20].

3. Influence of the second harmonic of the driving

From the symmetry considerations it follows that the long-time averaged velocity v of the Brownian motor is equal to zero if it is driven only by one harmonic, i.e. when $\varepsilon = 0$ in Eq. (6). In order to generate a directed motion of the motor, one has to include the second harmonic. Therefore we pose here the question: what is the influence of the second component ($\varepsilon \neq 0$) of the external force $g(t)$ on transport properties of the Brownian particle described by Eq. (4).

Nonlinearity and three-dimensional phase space $(x, y = \dot{x}, z = \omega t)$ make the system (4) possible to behave chaotically in the deterministic case ($D_0 = 0$). Many features depend strongly on the shape of basins of attraction. If we however plug the temperature on, it is very likely that we destroy the present scene of attractors and release the possibility for the system to proceed not only with attractors but more importantly with the deterministic unstable orbits. This situation is extremely complicated and can change from point to point in the five-dimensional parameter space $\{\gamma, \omega, a, \varepsilon, D_0\}$. It is almost impossible to find all features for such a system; therefore the goal of this work is focused only on the generic influence of the biharmonicity parameter ε. In fact, one is able to tangle the picture even more by setting the frequency of the second harmonic in $g(t)$ free, but authors feel that this is unnecessarily in this very work.

In the following we will fix the dimensionless temperature to the value $D_0 = 0.001$ and focus on the stochastic (not deterministic) properties.

3.1. Numerical experiment

In order to establish the influence of the second harmonic of the driving force on transport properties we have carried out comprehensive numerical simulations. We have employed Stochastic Runge–Kutta algorithm of the 2nd order with the time step of $[10^{-3}-10^{-4}](2\pi/\omega)$. All numerical calculations have been performed using CUDA environment on desktop computing processor NVIDIA Tesla C1060. This gave us a possibility to speed the numerical calculations up to few hundreds times more than on typical modern CPUs. More details on this very efficient method can be found in the work [21].

We focus on the asymptotic current or long-time averaged velocity v of the Brownian particle. Averaging was performed over 10^3-10^6 different realizations and over one period of the external driving force $T = 2\pi/\omega$. We choose all initial positions and velocities to be uniformly distributed over one potential period $[0,1]$ and the interval $v \in [-2,2]$, respectively.

3.2. Role of symmetry in time domain

Properties of the time dependent driving force $g(t)$ in Eq. (6) determine whether the Brownian particle is transported in the long-time regime, i.e. whether $v = 0$ or $v \neq 0$. We can distinguish two special cases of the force $g(t)$.

(i) The first case is when there is such t_0 that $g(t_0 + t) = g(t_0 - t)$. It means that the driving is symmetric or invariant under the time-inversion transformation, see solid and dotted lines in Fig. 1.
(ii) The second case is when there is such t_1 that $g(t_1 + t) = -g(t_1 - t)$. This is the case of the antisymmetric driving, see dashed and dotted-dashed lines in Fig. 1.

As a consequence, in the symmetric case (i), the stationary average velocity tends to zero when the friction coefficient γ tends to zero: $v \to 0$ when $\gamma \to 0$; if $\gamma \neq 0$ then generically $v \neq 0$. It is illustrated in Fig. 2 for $\phi = \pi/2, 3\pi/2$. In the asymmetric case (ii), the stationary average velocity tends to zero when the friction coefficient γ tends to infinity (the overdamped regime): $v \to 0$ when $\gamma \to \infty$; if $\gamma < \infty$ then generically $v \neq 0$. Let us note that contrary to the symmetric driving, for $\gamma \to 0$ the velocity $v \neq 0$, cf. Fig. 2. So, it means that the transport is generated by deterministic dynamics.

We consider the case of the symmetric driving with $\phi = \pi/2$ for the biharmonicity $\varepsilon = 0.5$ (see Fig. 1) and study the role of dissipation characterized by the friction coefficient γ. This is the case when for $\gamma = 0$ the stationary average velocity $v = 0$. When the friction coefficient increases starting out from zero, the average velocity becomes non-zero as is illustrated in Fig. 2. The average velocity as a function of γ displays non-monotonic dependence exhibiting maxima and minima. Moreover, it passes through zero and the current reversal phenomena can be detected. Because for $\gamma = 0$ the velocity $v = 0$ and for $\gamma \neq 0$ generically the velocity

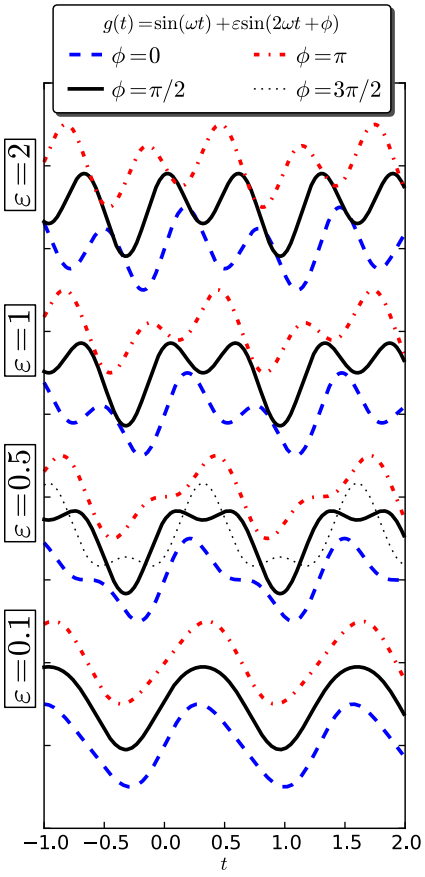

Fig. 1. Dimensionless external ac driving $g(t) = a[\sin(\omega t) + \varepsilon \sin(2\omega t + \phi)]$ for the fundamental amplitude $a = 1$, four different relative amplitudes of the second harmonics: $\varepsilon = 0.1, 0.5, 1, 2$ and selected values of the relative phase: $\phi = 0$ (blue dashed), $\pi/2$ (black solid), π (red dotted-dashed) and $3\pi/2$ (black dotted). For arbitrary values of a and ε, the ac driving possesses the time reflection symmetry for $\phi = \pi/2$ and $\phi = 3\pi/2$. For $\phi = 0$ and $\phi = \pi$ the driving is antisymmetric. For other values of the relative phase ϕ the driving is asymmetric. (For interpretation of the references to color in this figure legend, the reader is referred to the web version of this article.)

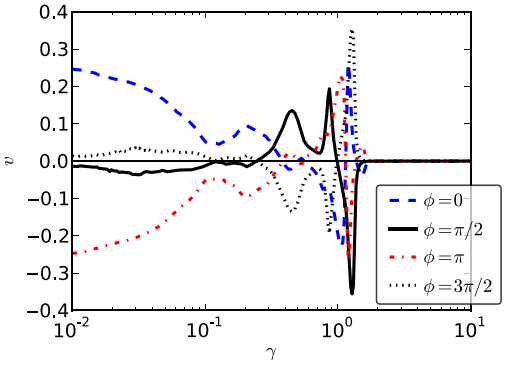

Fig. 2. The stationary average velocity v as a function of the friction coefficient γ is depicted for selected values of the relative phase ϕ. For $\phi = \pi/2, 3\pi/2$ the driving is symmetric while for $\phi = 0, \pi$ it is antisymmetric. Other parameters read: $a = 4.2, \omega = 4.9, \varepsilon = 0.5$ and $D_0 = 0.001$.

$v \neq 0$, this case is called the dissipation-induced symmetry breaking [22]: the coupling to thermal bath is enough to break the time-inversion symmetry. We note that for a fixed damping γ, the average velocity for the phase $\phi = 3\pi/2$ takes exactly the opposite sign to the case $\phi = \pi/2$.

Now, let us consider the antisymmetric case $\phi = 0$. For $\gamma = 0$, the velocity $v \neq 0$. The weak dissipation diminishes the stationary velocity in comparison to the dissipationless case. The dependence $v(\gamma)$ is also non-monotonic with minima and maxima. As in the symmetric case, the case with the phase $\phi = \pi$ can be obtained from the case $\phi = 0$ by the relation $v(\phi = \pi) = -v(\phi = 0)$.

3.3. Arbitrary shape of driving

In previous subsection we focused on specific values of the phase. Here we present the numerical investigation of the 3D parameter space $\{\phi, \varepsilon, \gamma\}$. For phases different than just mentioned above, we reveal also asymmetric external biharmonic signals. In the Fig. 3, the average velocity is presented in color plots for four different damping constants $\gamma = 0.01, 0.1, 0.9, 2$ (panels a–d respectively) and additionally for the overdamped limit (panel e). On the abscissa we vary the amplitude ε of the second component of the signal $g(t)$ and on ordinate we present phase $\phi \in [0, 2\pi]$. Light colors denote positive average velocity. Color becomes darker for values of v close to zero and eventually turn to dark-gray and black for negative valued average velocities.

For the weak friction the average velocity has reflection symmetry $v(\pi + \phi) = v(\pi - \phi)$ as we would expect from a system prepared very close to the limit of the frictionless or Hamiltonian systems, because then the relation $v \approx \sin(\phi + \pi/2)$ is quite well satisfied [23]. We plotted black dotted lines on each panel to guide the reader to the point where the driving force $g(t)$ possesses the reflection symmetry, i.e., for $\phi = \pi/2$ and $3\pi/2$.

As we increase the friction coefficient system loses its previous symmetry and becomes non-symmetric as one can easily see on panels (b) and (c). In other words – in the situation where both characteristic times in the system τ_γ and the period T of the driving take more or less the same value, the battle between periodic stimulation and damping (not strong enough to suppress the driving influence quickly with possibility of additional energy cumulation) causes the whole irregular dynamics as seen on the central panel (c) of Fig. 3. If we, however, analyze situation with strong damping the picture again gains the symmetry but now of a different kind, i.e. $v(\pi + \phi) = -v(\pi - \phi)$, cf. panel (e) in Fig. 3. The close inspection of all case presented in Figs. 2 and 3 leads to the important conclusion that for a fixed set of all parameters, there is the shift symmetry of the stationary velocity with respect to the phase, i.e.,

$$v(\phi) = -v(\phi + \pi). \tag{7}$$

This relation is a particular case of a more general relation

$$v(-\varepsilon) = -v(\varepsilon), \tag{8}$$

which follows from the symmetry considerations. One can note that the transformation $\phi \to \phi + \pi$ is equivalent to the transformation $\varepsilon \to -\varepsilon$. The same relation holds true if, instead of the second harmonics, we apply a constant force F. Then of course $v(-F) = -v(F)$ [6]. Remember that for any set of parameters the stationary average velocity $v = 0$ when $F = 0$ or $\varepsilon = 0$.

3.4. Controlling transport by symmetric signals

We analyze the case when the external driving is symmetric. We set the phase of the second harmonics to $\phi = \pi/2$ (see black solid curves in Fig. 1). We check the system response to the signal against the relative amplitude of the second harmonics ε for the range starting from 0 and ending at the value higher than doubled base driving amplitude a. In Fig. 4 these characteristics are plotted for selected driving frequencies $\omega = 0.1, 3, 4, 4.9$. From numerical analysis it follows that the average velocity changes its sign by varying the parameter ε for all inspected frequencies of the external driving. It means that the shape of the external signal

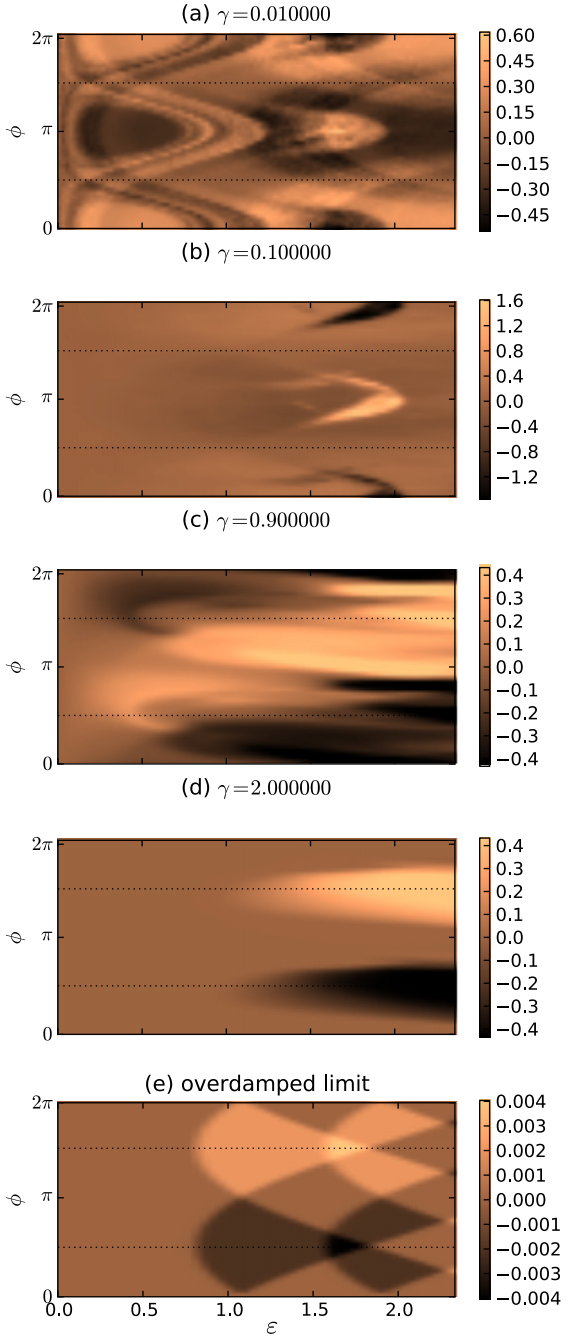

Fig. 3. Influence of the second harmonic of the external force $g(t)$ on transport properties of the system (4). Dependence of the drift velocity on both the relative amplitude ε (horizontal axis) and the relative phase ϕ (vertical axis) is depicted for various damping constants $\gamma = 0.01, 0.1, 0.9, 2.0$ and for the overdamped limit (top to bottom). Other parameters are: $a = 4.2, D_0 = 0.001$ and $\omega = 4.9$. Black dotted lines are plotted on all panels showing the phases for which the driving force $g(t)$ possesses the reflection symmetry $t \to -t$, i.e. for $\phi = \pi/2$ and $3\pi/2$.

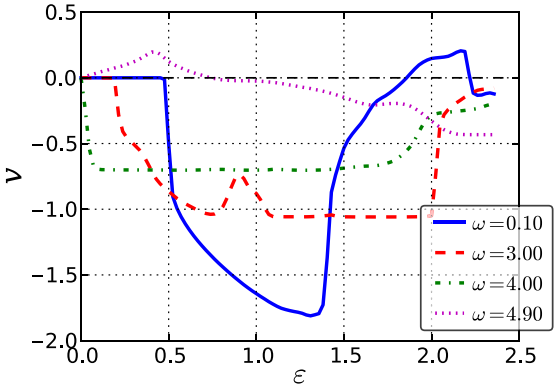

Fig. 4. The stationary averaged velocity *vs.* the relative amplitude ε of the second harmonics for four values of the angular frequency ω of the signal $g(t)$. Other parameters are: $a = 4.2, \gamma = 0.9, \phi = \pi/2$ and $D_0 = 0.001$.

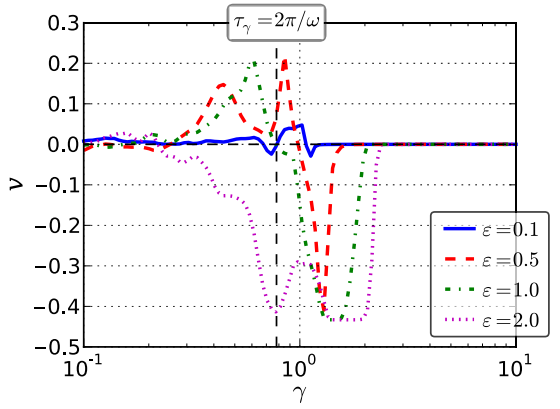

Fig. 5. Logarithmic dependence of the average velocity on the friction coefficient γ is plotted for four relative amplitudes ε of the second harmonics of the external driving $g(t)$. Vertical black dashed line marks the point of the critical value of the friction coefficient, for which two characteristic times, relaxation time of the velocity $\tau_\gamma = 1/\gamma$ and period $T = 2\pi/\omega$ of the driving force, are equal. One can easily notice rich behavior of the average velocity around this specific value. Other parameters are: $a = 4.2, \omega = 4.9, \phi = \pi/2$ and $D_0 = 0.001$.

can control values and direction of the net velocity in the system. The current reversal can be multiple ($\omega = 0.1$), akin to the situation described in [24]. Keeping ε constant at a certain level usually the direction of the average motion of Brownian particles changes its sign for the different values of the driving frequency ($\varepsilon = 0.5$ or 2.0). On the contrary there are regimes within the scanned parameter space $\{\varepsilon, \omega\}$ where regardless the values of ω chosen the system response is qualitatively the same.

Next we explore the transport properties for the Brownian particle moving in the viscous environment with different friction coefficients. We examine the character of the system response against the signal of the different shape which we can control by tuning the parameter ε(see Fig. 1 for details). There are two alternative limits for the viscous system behavior – Hamiltonian where system is frictionless [25–27] and overdamped where the characteristic relaxation time for the velocity $\tau_\gamma = 1/\gamma$ is very long. Between those two peripheries there is a region of moderate damping which seems to be the most intriguing [5,6,28,29]. It provides rich spectrum of the very interesting phenomena and therefore we are going to focus on this particular domain in the following.

In Fig. 5 the reflection of the impact of different shapes and strengths of external driving for the friction constant γ in the range from 0.1 to 10 can be found. This means that the characteristic relaxation time passes from 10 to 0.1. If we refer this time to the second characteristic time of importance for system (4), namely the period of the external driving $T = 2\pi/\omega \simeq 1.28$, one can see that the point where both characteristic times are of the same order can be identified more or less in the middle of the chosen region of analyzed damping constants. Indeed, after examining of Fig. 5, one can easily reveal most exciting features around essential value of the damping constant marked by the vertical dashed black line on the plot. At low friction, the average velocity is close to zero. When we, however, increase the friction coefficient to the value of

around $\gamma = 0.3$ the system starts to react in a different way depending on the relative strength of the second harmonic ε. For strengths less then or equal to 1 the current becomes positive, while for $\varepsilon = 2$ system reacts with the opposite sign. This gives a possibility to control the transport simply by varying the strength of the second source of the external field. When we go even further and arrive to the vicinity of the critical point $\tau_\gamma = 2\pi/\omega$, the previous positive valued current starts to drop, crosses zero and becomes negative quite steeply. Surprisingly values of average velocities for all strengths higher than 0.5 possess almost the same negative values just above $\gamma = 1$. Additional enlargement of the friction leads to reduce of the transport possibilities of the system. It does not reach zero, but decreases of several orders of magnitude – see panel (e) in Fig. 3 for details. By setting the strength to zero we end up with the antisymmetric force and with zero current for any value of the friction constant due to the symmetry reasons.

4. Summary

We have explored transport properties of the Brownian particles in a symmetric potential, driven by the time-periodic biharmonic signals. We have demonstrated how the symmetry of driving force influences the transport features. There exists two limits: overdamped and frictionless. It turns out that in those two limits different types of symmetry exclude transport. In the frictionless case the system is time-reversible, thus the symmetric driving cannot distinct the direction. On the other hand, in the case of overdamped motion the antisymmetric driving leads to zero current. In all other cases, as the Curie principle suggests, the particle has generally non-zero average velocity. The closer inspection shows that the magnitude and sign of the current has complex structure in the parameter space. Typically, the multiple current reversals occur, when one of the system parameters is changed.

In this paper, thermal noise $\xi(t)$ in Eq. (2) is assumed to be white noise of zero correlation time. In real systems the correlation time of thermal fluctuations is never zero. In many situations this approximation is very well but there are also situations where the white-noise approximation fails and a different treatment based e.g. on the generalized Langevin equation should be used [30]. However, it is essentially beyond the scope of the paper and requires separate investigations.

Finally, let us remind that the Langevin equation (2) has similar form as an equation of motion for the phase difference $\Psi = \Psi(t)$ between the macroscopic wave functions of the Cooper pairs on both sides of the Josephson junction. The quasi-classical dynamics of the resistively and capacitively shunted Josephson junction, which is well known in the literature as the Stewart–McCumber model [8,9,11], is described by the following equation

$$\left(\frac{\hbar}{2e}\right)^2 C\ddot{\Psi} + \left(\frac{\hbar}{2e}\right)^2 \frac{1}{R}\dot{\Psi} + \frac{\hbar}{2e} I_0 \sin\Psi = \frac{\hbar}{2e} I(t) + \frac{\hbar}{2e}\sqrt{\frac{2k_BT}{R}}\xi(t). \quad (9)$$

The left hand side contains three additive current contributions: a displacement current due to the capacitance C of the junction, a normal (Ohmic) current characterized by the normal state resistance R and a Cooper pair tunnel current characterized by the critical current I_0. In the right hand side, $I(t)$ is an external current. Thermal fluctuations of the current are taken into account according to the fluctuation–dissipation theorem and satisfy the Nyquist formula associated with the resistance R. It is an evident correspondence between two models: the coordinate $x = \Psi - \pi/2$, the mass $m = (\hbar/2e)^2 C$, the friction coefficient $\gamma = (\hbar/2e)^2(1/R)$, the barrier height $\Delta V = (\hbar/2e)I_0$ and the period $L = 2\pi$. The biharmonic signal $G(t)$ in Eq. (1) corresponds to the external current $I(t)$. The velocity $v = \dot{x}$ corresponds to the voltage V across the junction. So, all transport properties can be tested in the setup consisting of a resistively and capacitively shunted Josephson junction device.

Acknowledgment

The work supported in part by the MNiSW Grant N202 203534 and the Foundation for Polish Science (L.M.). The authors thank M. Januszewski for preparing the precise program (http://gitorious.org/sdepy) that we have used for numerical calculations. We would like to acknowledge Peter Hänggi, our friend and mentor, for long-term collaboration, inspiring, motivating and never ending – not only scientific – discussions.

References

[1] L. Machura, M. Kostur, J. Łuczka, Biosystems 94 (2008) 253.
[2] P. Hänggi, F. Marchesoni, Rev. Mod. Phys. 81 (2009) 387.
[3] H. Linke (Ed.), Ratchets and Brownian motors: basics, experiments and applications, Appl. Phys. A 75 (2002).
[4] J. Łuczka, R. Bartussek, P. Hänggi, Europhys. Lett. 31 (1995) 431;
T. Czernik, J. Kula, J. Łuczka, P. Hänggi, Phys. Rev. E. 55 (1997) 4057;
J. Kula, M. Kostur, J. Łuczka, Chem. Phys. 235 (1998) 27.
[5] L. Machura, M. Kostur, P. Talkner, J. Łuczka, P. Hänggi, Phys. Rev. Lett. 98 (2007) 040601.
[6] M. Kostur, L. Machura, P. Talkner, P. Hänggi, J. Łuczka, Phys. Rev. B 77 (2008) 104509;
M. Kostur, L. Machura, J. Łuczka, P. Talkner, P. Hänggi, Acta Phys. Polon. B 39 (2008) 1177.
[7] J. Nagel, D. Speer, T. Gaber, A. Sterck, R. Eichhorn, P. Reimann, K. Ilin, M. Siegel, D. Koelle, R. Kleiner, Phys. Rev. Lett. 100 (2008) 217001.
[8] W.C. Stewart, Appl. Phys. Lett. 12 (1968) 277.
[9] D.E. McCumber, J. Appl. Phys. 39 (1968) 3113.
[10] A. Barone, G. Paternò, Physics and Application of the Josephson Effect, Wiley, New York, 1982.
[11] R.L. Kautz, Rep. Prog. Phys. 59 (1996) 935.
[12] P. Hänggi, H. Thomas, Phys. Rep. 88 (1982) 207.
[13] M. Borromeo, F. Marchesoni, Europhys. Lett. 72 (2005) 362.
[14] M. Borromeo, P. Hänggi, F. Marchesoni, J. Phys.: Condens. Matter 17 (2005) S3709.
[15] M. Borromeo, F. Marchesoni, Phys. Rev. E 73 (2006) 016142.
[16] H.J. Breymayer, Appl. Phys. A 33 (1984) 1.
[17] F. Renzoni, Cont. Phys. 46 (2005) 161.
[18] M. Brown, F. Renzoni, Phys. Rev. A 77 (2008) 033405.
[19] S. Denisov, S. Flach, P. Hänggi, Nonlinearities in periodic structures and metamaterials, in: C. Denz, S. Flach, Y. Kivshar (Eds.), Springer Series in Optical Sciences, vol. 150, Springer, 2010, pp. 181–190.
[20] R. Monaco, J. Appl. Phys. 68 (1990) 679.
[21] M. Januszewski, M. Kostur, Comput. Phys. Commun. 181 (2010) 183.
[22] R. Gommers, S. Bergamini, F. Renzoni, Phys. Rev. Lett. 95 (2005) 073003.
[23] O. Yevtuschenko, S. Flach, Y. Zolotaryuk, A.A. Ovchinnikov, Europhys. Lett. 54 (2001) 141.
[24] M. Kostur, J. Łuczka, Phys. Rev. E 63 (2001) 021101.
[25] H. Schanz, M.F. Otto, R. Ketzmerick, T. Dittrich, Phys. Rev. Lett. 87 (2001) 070601.
[26] S. Denisov, S. Flach, P. Hänggi, Europhys. Lett. 74 (2006) 588.
[27] R. Salgado-Garca, M. Aldana, G. Martnez-Mekler, Phys. Rev. Lett. 96 (2006) 134101.
[28] L. Machura, M. Kostur, F. Marchesoni, P. Talkner, P. Hänggi, J. Łuczka, J. Phys.: Condens. Matter 17 (2005) S3741.
[29] Bao-quan Ai, Liang-gang Liu, Phys. Rev. E 76 (2007) 042103.
[30] M. Kostur, J. Łuczka, P. Hänggi, Phys. Rev. E 80 (2009) 051121.